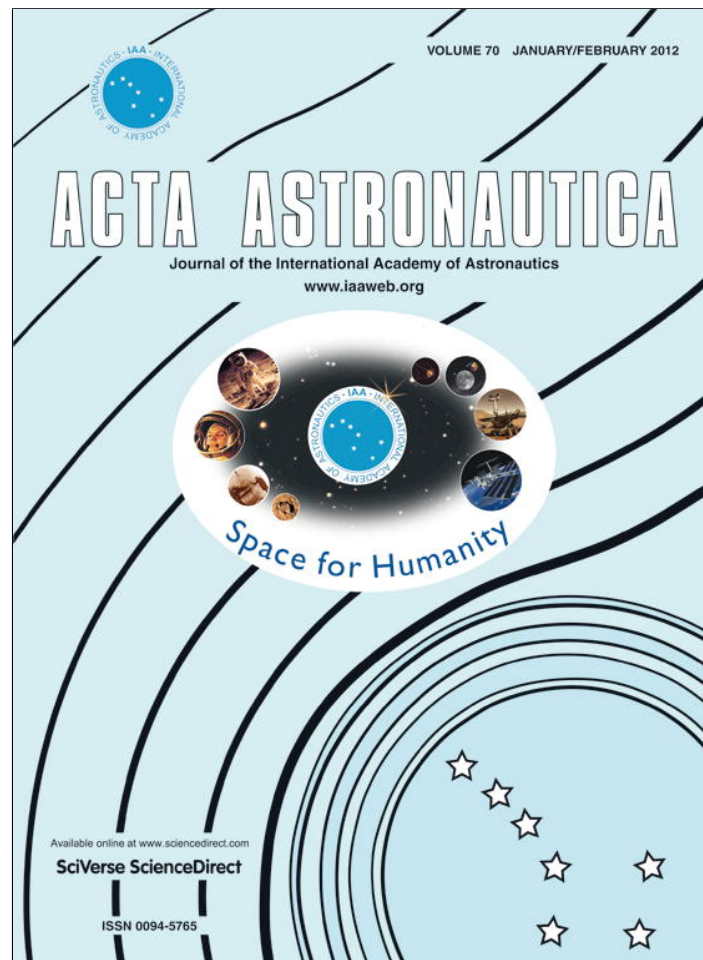


Provided for non-commercial research and education use.
Not for reproduction, distribution or commercial use.



(This is a sample cover image for this issue. The actual cover is not yet available at this time.)

This article appeared in a journal published by Elsevier. The attached copy is furnished to the author for internal non-commercial research and education use, including for instruction at the authors institution and sharing with colleagues.

Other uses, including reproduction and distribution, or selling or licensing copies, or posting to personal, institutional or third party websites are prohibited.

In most cases authors are permitted to post their version of the article (e.g. in Word or Tex form) to their personal website or institutional repository. Authors requiring further information regarding Elsevier's archiving and manuscript policies are encouraged to visit:

<http://www.elsevier.com/copyright>

Contents lists available at SciVerse ScienceDirect

Acta Astronautica

journal homepage: www.elsevier.com/locate/actaastro

Study on the eddy current damping of the spin dynamics of space debris from the Ariane launcher upper stages

N. Praly^{a,*}, M. Hillion^a, C. Bonnal^b, J. Laurent-Varin^c, N. Petit^d

^a SYSNAV, 57 Rue de Montigny, 27200 Vernon, France

^b CNES, DLA, 52 rue Jacques Hillairet, 75612 Paris Cedex, France

^c CNES, DCT/SI/GS, 18 avenue Edouard Belin, 31401 Toulouse Cedex 4, France

^d MINES ParisTech, CAS, 60-62 Boulevard Saint Michel, 75272 Paris Cedex 06, France

ARTICLE INFO

Article history:

Received 15 September 2011

Received in revised form

2 March 2012

Accepted 4 March 2012

Keywords:

Space debris

Eddy currents

Damping of spin motion

ABSTRACT

This paper addresses the topic of damping of the spin dynamics of a spatial debris orbiting around the Earth. Such debris, which can consist of parts of heavy launchers such as the Ariane rocket under consideration in this article, are impacted by torques generated by eddy currents as their conducting non-ferromagnetic body orbits through the Earth magnetosphere. Several previous works have focused on describing this induction phenomenon and have proposed analysis of empirical observations of this particular and important effect which has attracted much attention since the number of spatial debris has emerged as a problem for the future of space programs, especially in low orbits. In this paper, we present a relatively comprehensive modeling of the induction phenomenon, by means of Maxwell's equations inside the conducting and non-ferromagnetic body. Through the generalized Ohm's law, we show how one can obtain a partial differential equation with Neumann's boundary conditions problem that, once solved, e.g. through a finite elements method, yields the values of induced currents and braking torques. The case of a depleted upper stage of a heavy launcher, having a cylindrical shape and thin walls is particularly studied. We show a methodology to estimate the decay-rate of the spinning velocity, which is proven to satisfy a first-order asymptotically stable linear dynamics. Special cases consisting of typical orbit of space debris are treated.

© 2012 Elsevier Ltd. All rights reserved.

1. Introduction

The number of man-made space debris orbiting around the Earth has steadily increased since the early days of space programs. It seems that a critical point has been reached in 2007 after the orbital explosion of the Chinese satellite ASAT which was followed, in 2009, by the collision of the Iridium

33 satellite and Cosmos 2251 stage. These incidents are reported to have generated more than 1300 debris of various sizes and shapes [19]. Furthermore, future collisions between debris are expected to generate an increasing number of smaller debris and significantly raise the risks of damaging impacts on satellites and other spacecrafts, especially in low orbits. This problem has spurred a recent and strong interest for developing debris deorbiting technologies, in hope of alleviating the risk by removing, at least, the largest or the most dangerous debris. Various candidate solutions have been proposed. The vast majority of them consider the capture of the debris by a chaser prior to the deorbiting. In particular, nets [20], tethers [7], solar sails [10] and boosters [13] have been considered. Most of these

* Corresponding author. Tel.: +33 232641240.

E-mail addresses: nicolas.praly@sysnav.fr (N. Praly),
mathieu.hillion@sysnav.fr (M. Hillion),
christophe.bonnal@cnes.fr (C. Bonnal),
julien.laurent-varin@cnes.fr (J. Laurent-Varin),
nicolas.petit@mines-paristech.fr (N. Petit).

proposed techniques have obvious difficulties in capturing rapidly rotating objects. Indeed, it is quite difficult to attach a tether device to a spinning body, and catching a spinning debris with a net can turn out to be troublesome, especially in flat spin mode [16].

Interestingly, the effects of the Earth magnetic field can help here. At each instant, the permanent magnetic field from the magnetosphere generates eddy currents in the rotating, conducting body. These induction-created currents generate, in turn, a torque opposed to the rotation of the body. Then, one can expect the initial rotation to damp over time, and eventually, asymptotically stabilize to zero. This article describes a method to establish the damped dynamics of the debris in rotation, around one of its principal axes, in Earth orbit. The shape under consideration can be relatively general, but the case we focus on is a thin-wall cylindrical body, closed at the two ends by thin-wall half-spheres (we call this shape “capsule”). It is a representative for the debris stemming from the upper stage of the heavy launcher Ariane.

To model eddy currents, we start from Maxwell's equations and consider the generalized Ohm's law to relate the density of current to the external magnetic field. Using the obtained equation inside and on the boundary of the conducting body (which is assumed to be non-ferromagnetic and not the subject of self-induction), we formulate a general partial differential equations with Neumann's boundary conditions problem in the electric potential variable. This problem can be solved numerically in general and analytically in simple cases. From the electric potential inside the conducting body, one can deduce the density of induced currents, from which the braking torque can be computed. In general, the spin dynamics takes the form of a first-order asymptotically stable linear differential equation in the rotation velocity variable. The damping rate is numerically determined through the previously discussed method. The study is complemented by integrating this damped equation along orbits of reference, which defines the orientation and the strength of the exerted magnetic field. This serves to estimate the decay-rate of the initial spin, for various orbits and various size of debris.

The paper is organized as follows. In Section 2, we give a brief overview of the literature on space debris, showing the risk of collision that they generate, the nature of the debris, their number and their density in various parts of the near-space domain. We also give an outlook on the currently envisioned deorbiting and capture technologies. In Section 3, we formulate the discussed Neumann problem for such a conducting debris. The example of capsule bodies is illustrated. We also explain how this problem can be numerically treated with a finite-element solver. Examples of the obtainable accuracy are given, for particular cases of conducting bodies where an analytic solution exists, e.g. a rotating sphere. In Section 4, we establish the damped differential equation and solve it along orbits and for bodies of particular interest. Numerical results pertaining to typically Ariane launcher upper stages are reported.

2. The problem of space debris

Since the beginning of the space conquest in 1957, human space activity has produced a large amount of

debris. The origins of those objects are quite various: sources range from out of service satellites to objects produced by launch missions (last stages of launch vehicles and separation devices to name a few). Currently, more than 15,500 debris are cataloged in low Earth orbit (debris larger than 10 cm [12]). Most of them orbiting in the same orbits as satellites in use. Unfortunately, debris are very dangerous, as a debris larger than 1 mm can cause critical damage to a satellite. Even if most of the recent spacecrafts have avoidance capabilities, such procedures cannot be used for debris smaller than 10 cm because the debris cannot be detected, orbit determination and thus collision prediction are not possible.

Nearly 20 years ago, a first article was published on the risk of cascading effects due to collisions between debris in low Earth region. At that time, this phenomenon, since named the “Kessler Syndrome” [9], was not considered as a serious threat. Today, due to multiple collisions between orbital bodies, this effect is well accepted and space agencies over the world are now cooperating to develop mitigation strategies. The current situation is, in some aspects, relatively alarming because our ability to use outer space is jeopardized in the long run. New guidelines and recommended practices have been set to limit the lifetime of objects in outer space, but older debris which are already in stable orbits will remain there and eventually produce more debris through collisions. Simulations have shown that the situation cannot be improved unless some of the debris are actually removed [12]. Reducing the number of objects is now a necessity to ensure the sustainability of future space activities. The most polluted area is the low Earth orbit. The removal must begin with massive objects which have the largest collision probabilities, typically vehicle stages and out-of-service satellites. The shape of those objects is well-known and offers a solid mechanical interface which is advantageous if catching is considered. On the other hand, attitudes of these debris are not known and the current technologies do not allow to catch objects which rotate faster than a few degrees per second. Launcher upper stages are usually passivated at the end of their life in order to reduce the risk of explosion due to overpressure in their fuel tanks, but this venting potentially imparts to the stage of an angular rotation which can reach a few tens of degrees per second; such high values would probably represent a major obstacle to the capture of the stage with current technologies. Several of the most promising solutions baseline the capture of the debris with a robotic arm before equipping it with a deorbitation kit such as an electrodynamic tether [7], a drag augmentation surface or a solar sail [10]. Other conceivable solutions use a spacetug to push or pull the debris in the Earth atmosphere without using a robotic arm, but nevertheless with prior control of the debris dynamics. Finally, one can note that even contactless solutions such as the use of laser beam to “push” or “destroy” the object may be strongly perturbed by a high rotation speed of the debris. For the vast majority of the conceivable solutions, high angular velocities represent a limiting factor, unfortunately, rendering the most promising concepts impractical.

Since 1957, observations on the rotation period have been made for satellites and rocket bodies. Various studies [17,1] have shown that the rotation period exponentially

increases over time. The increase stems from various factors: friction due to the remaining fuel contained in the tanks, air drag (for trajectories having altitude below 500 km) and, interestingly, eddy currents torque. This phenomenon is of great importance for any future “catching mission” because, even if a debris has a high rotation speed at the beginning of its life, the rotation will decrease over time. A critical question naturally emerges: how to evaluate the damping time constant. The answer will be given in this paper for Ariane 4 H10 stages.

To determine the decay time, we study the eddy current torque induced in a debris rotating in the Earth magnetic field. For simple shapes eddy currents torques have already been calculated under the form of analytic formulas. The case of a spherical body is treated in the historical article of Hertz [4], while a spherical body with self-induction is addressed in [15]. A hollow cylinder is considered in [14]. Modern numerical tools allow to consider more general cases. The methodology that we advocate in this article can be extended to complex shapes and various types (e.g. altitude, inclination) of orbits.

3. Equations governing the magnetic induction phenomenon inside a spinning conduction non-ferromagnetic body

Induction can be described by Maxwell's equations, involving the potential associated to the electric and magnetic fields, the expression of the Lorentz force and Ohm's law. The nomenclature we use is found in Table 1.

Table 1
Nomenclature.

Symb.	Quantity	Unit
$\vec{E}(M,t)$	Electric field	V m ⁻¹
$\vec{B}(M,t)$	Magnetic field	T or G
$\rho(M,t)$	Total charge density	C m ⁻³
$\vec{j}(M,t)$	Total current density	A m ⁻²
$V(M,t)$	Electric potential	V
$\vec{A}(M,t)$	Magnetic vector potential	T m
$\kappa(M,t)$	Resistivity of a material	Ω m
q	Charge of a particle	C
μ_0	Permeability of free space	H m ⁻¹
ϵ_0	Permittivity of free space	C V ⁻¹ m ⁻¹
ω	Angular velocity	°/s or rad s ⁻¹
$\vec{\omega}$	Angular velocity vector ($=(\omega_i, \omega_j, \omega_k)$)	°/s or rad s ⁻¹
$\vec{v}(M,t)$	Velocity	m s ⁻¹
$\vec{F}(M,t)$	Lorentz force	N
$\vec{T}(M,t)$	Torque	N m
\vec{I}	Inertia tensor	kg m ²
Ω	Volume of a conducting material	m ³
Ω_s	Surface of a conducting material	m ²
$d\Omega$	Mesoscopic volume	m ³
dS	Infinitesimal area of surface	m ²
M	Point of interest	–
P	Point of interest on Ω_s	–
$\vec{n}(P)$	Normal vector to Ω_s	–
O	Origin of the reference frames	–
$G(M, M_0)$	Green's function	–
$-f$	Vector/coordinate written in fixed frame	–
$-b$	Vector/coordinate written in body frame	–

3.1. Fundamental equations

Before formulating the problem of induction, we introduce the fundamental equations used throughout the analysis: under the assumption of small variation in time, Maxwell's equations at the point M read

$$\vec{\nabla} \cdot \vec{E}(M,t) = \frac{\rho(M,t)}{\epsilon_0} \quad (1)$$

$$\vec{\nabla} \cdot \vec{B}(M,t) = 0 \quad (2)$$

$$\vec{\nabla} \times \vec{B}(M,t) = \mu_0 \vec{j}(M,t) \quad (3)$$

$$\vec{\nabla} \times \vec{E}(M,t) = -\frac{\partial \vec{B}(M,t)}{\partial t} \quad (4)$$

The charge conservation $\vec{\nabla} \cdot \vec{j}(M,t) = 0$ is consistent with the previous Maxwell's equations (we assume that there is no charge created inside the conducting material). The properties of the electromagnetic field enable us to introduce the electric potential and magnetic vector potential

$$\vec{E}(M,t) = -\vec{\nabla}(V(M,t)) - \frac{\partial \vec{A}(M,t)}{\partial t} \quad \text{and} \quad \vec{B}(M,t) = \vec{\nabla} \times \vec{A}(M,t) \quad (5)$$

We also introduce the Lorentz force

$$\vec{F} = q(\vec{E}(M,t) + \vec{v} \times \vec{B}(M,t)) \quad (6)$$

With Eqs. (5) and (6), the generalized Ohm's law is

$$\kappa \vec{j}(M,t) = -\vec{\nabla}(V(M,t)) - \frac{\partial \vec{A}(M,t)}{\partial t} + \vec{v}(M,t) \times \vec{B}(M,t) \quad (7)$$

3.2. Typical induction problem

Consider a volume Ω in which each point M of Ω moves at speed $\vec{v}(M,t)$ with respect to an inertial reference frame, through a constant magnetic field. Moreover, assume that the self-induction phenomenon is negligible and that the only surrounding magnetic field is the stationary Earth magnetic field. Assume that the magnetic field is spatially homogeneous (constant with respect to the space variable) at the scale of an object and time invariant, so $\vec{B}(M,t) = \vec{B}_0$. The current inside this volume satisfies Ohm's law (7). For a stationary magnetic field, this equation yields

$$\kappa \vec{j}(M,t) = -\vec{\nabla}(V(M,t)) + \vec{v}(M,t) \times \vec{B}_0 \quad (8)$$

The current inside Ω satisfies two conditions

1. $\vec{\nabla} \cdot (\vec{j}(M,t)) = 0, \forall M \in \Omega$ (charge conservation),
2. $\vec{j}(P,t) \cdot \vec{n}(P) = 0, \forall P \in \Omega_s$ (the currents remain inside the volume).

To determine the current inside Ω , one has to find the potential $V(M)$. The two previous properties, applied to the simplified Ohm's law (8), define a typical Neumann problem

$$\begin{cases} \Delta V(M) = F(M) & \forall M \in \Omega \\ \left. \frac{\partial V(P)}{\partial n} \right|_{\Omega_s} = f(P) & \forall P \in \Omega_s \end{cases} \quad (9)$$

Formally, this problem could be solved through a Green's function. As is detailed in [11] and [2], Green's

function $G(M, M_0)$ is unique and is defined by the following mathematical properties:

1. G is harmonic in Ω except at the fixed point M_0 , near which G is of the form

$$G(M, M_0) = \frac{1}{4\pi |MM_0|} + \text{a regular function} \quad (10)$$

2. $\frac{\partial G}{\partial n} = \frac{1}{S_0}$ (11)

where S_0 is the area of the surface Ω_s

3. $\int_{\Omega_s} G \, dS = 0$ (12)

The potential solution of problem (9) is then

$$V(M_0) = - \int_{\Omega} G(M, M_0) f \, d\Omega - \int_{\Omega_s} G(P, M_0) f(P) \, dS + \text{constant} \quad (13)$$

The solution to Eq. (9) is unique up to a constant which, classically, is of little importance because it is its gradient which creates the current.

Once the current is known, the torque created by the current inside Ω is found through the expression of the Lorentz force (6). The torque created at a point A by an infinitesimal volume $d\Omega$ with a density current $\vec{j}(M, t)$ through a magnetic field $\vec{B}(M, t)$ is

$$d\vec{T} = \vec{AM} \times (\vec{j}(M, t) \times \vec{B}(M, t)) \cdot d\Omega \quad (14)$$

Summary: At the light of the previous discussion, let us now summarize the method to determine the torque created by eddy currents in a conducting material:

1. Formulate simplified Ohm's law (8) for the conducting material (in an inertial reference frame).
2. Apply the two properties (charge conservation, orthogonality of the current and the normal to the surface) of the current inside a conducting material to the simplified Ohm's law to get a typical Neumann problem on the electric potential (9), i.e. determine F and f .
3. Solve the Neumann problem (9).
4. Reformulate the simplified Ohm's law with the expression of the electric potential to find the current density in the material.
5. Evaluate the torque (14).

One critical point in this method is to solve the Neumann problem (9). In fact there are only few cases where the solution can be analytically determined. A sphere is one of the few geometries for which a simple analytical solution exists. We deal with this case in Section 3.3. Most of the time, a finite-elements method must be used. It enables one to solve this kind of problem for various body shapes. In particular, we use such method to evaluate the torque created by eddy current in a capsule in Section 3.4. As an analytical solution for spherical bodies is available [4], the finite-elements solver performance can be evaluated for the induction problem in Section 3.3.

3.3. Induction problem applied to a sphere or a spherical shell

Consider the following coordinate system:

- (e_x, e_y, e_z) a fixed coordinate system (f subscript), the origin O is the geometric center of the object.
- (e_i, e_j, e_k) a body coordinate system (b subscript), the origin O is the geometric center of the object.

With these notation, consider a spherical conducting body rotating along its Oz_f axis (the e_z axis and the e_k axis coincide). The rotation speed is $\vec{\omega} = \omega \vec{e}_z$ and the magnetic field $\vec{B}_f(M, t) = B(\sin \lambda \vec{e}_x + \cos \lambda \vec{e}_z)$ (Fig. 1). Define (j_x, j_y, j_z) the components of $\vec{j}_f(M, t)$ in Cartesian coordinates. Neglect the self-induction phenomenon. This problem has already been solved in 1880 by Hertz [4] who has provided an analytical formula reproduced in the following which will be used to cross validate the finite element solver we use (here FreeFEM [3]).

The torque (in the body reference frame) is

- for a sphere of radius R

$$\vec{T}_b = - \frac{2}{15} \pi \frac{B^2 \omega}{\kappa} \sin^2(\lambda) R^5 \vec{e}_k \quad (15)$$

- for a spherical shell of radius R and a thickness d

$$\begin{aligned} \vec{T}_b &= - \frac{2}{15} \pi \frac{B^2 \omega}{\kappa} \sin^2(\lambda) (R^5 - (R-d)^5) \vec{e}_k \\ &\approx \underbrace{- \frac{2}{3} \pi \frac{B^2 \omega}{\kappa} \sin^2(\lambda) d R^4}_{d \ll R} \vec{e}_k \end{aligned} \quad (16)$$

Comparisons of the above described finite element solver to those analytic formulas are reported in Table 2 for a spherical body of 1 m radius and the coefficient $(B^2 \omega / \kappa) \sin^2 \lambda = 1 \text{ N m}^{-4}$.

The difference between the two methods is negligible for our application. The finite element method and its solver are well suited to determine the torque created by eddy currents.

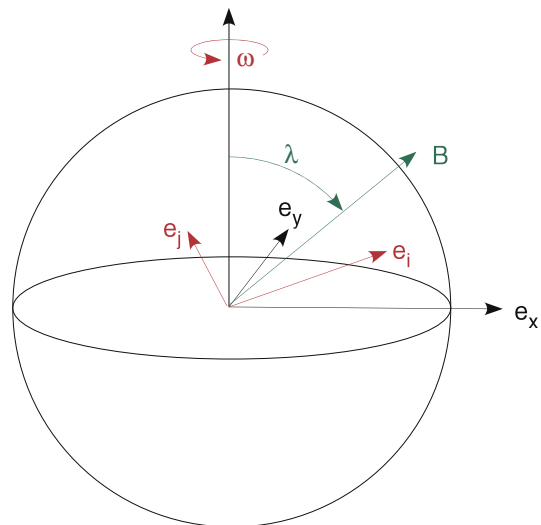


Fig. 1. Notations for a spherical body.

Table 2

Comparison between analytical and finite-elements results for a spherical body ($R=1$ m).

Thickness (mm)	Analytical result (mN m)	Finite element result (mN m)	Relative error (%)
5	10.37	10.32	0.4792
10	20.53	20.43	0.4888
20	40.22	40.06	0.4772
30	59.17	58.89	0.4870
Full	418.9	414.2	1.095

3.4. Induction problem applied to a capsule

The capsule is a thin-wall cylindric body closed at the two ends by thin-wall hemispheres. The length of the cylinder is L , its radius R and its thickness d . The two hemispherical shells have the same radius and thickness as the cylindrical part. To determine the torque induced by eddy currents two cases must be considered: the first case we study is the capsule rotating along its longitudinal axis, the second is the same capsule rotating along a transverse axis (flat spin) (Fig. 2).

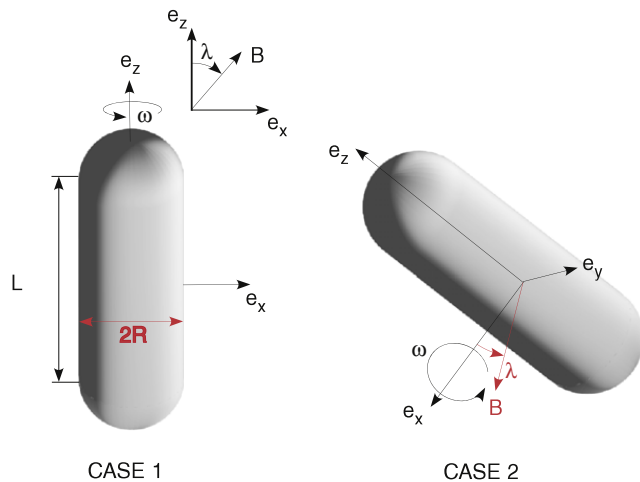


Fig. 2. Definition of the notations for a capsule rotating along its longitudinal axis and along its transverse axis.

Case1: capsule rotating along its longitudinal axis. We use the same systems of coordinates as for the sphere. The Oz_f axis is the longitudinal axis of the capsule. The rotation speed along this axis is ω ($\vec{v}_f = -\omega y_f \vec{e}_x + \omega x_f \vec{e}_y$). The magnetic field is $\vec{B}_f(M,t) = B(\sin \lambda \vec{e}_x + \cos \lambda \vec{e}_z)$. We define (j_x, j_y, j_z) the components of $\vec{j}_f(M,t)$ in Cartesian coordinates. Again, the self-induction phenomenon is neglected.

The methodology described in the previous sections is used:

1. From the simplified Ohm's law (8) for a rotating capsule, one gets

$$\begin{cases} \kappa j_x = -\frac{\partial V}{\partial x_f} + \omega x_f \cos \lambda B \\ \kappa j_y = -\frac{\partial V}{\partial y_f} + \omega y_f \cos \lambda B \\ \kappa j_z = -\frac{\partial V}{\partial z_f} - \omega x_f \sin \lambda B \end{cases} \quad (17)$$

2. The Neumann problem for a rotating capsule is

$$\begin{cases} \Delta V = 2\omega B \cos \lambda \\ x_f \frac{\partial V}{\partial x_f} + y_f \frac{\partial V}{\partial y_f} = \omega(x_f^2 + y_f^2) B \cos \lambda & \underbrace{r=R \text{ and } r=R-d}_{\text{cylindrical part}} \\ x_f \frac{\partial V}{\partial x_f} + y_f \frac{\partial V}{\partial y_f} + \left(z_f - \frac{L}{2}\right) \frac{\partial V}{\partial z_f} \\ = \omega(x_f^2 + y_f^2) B \cos \lambda - \omega \left(z_f - \frac{L}{2}\right) x_f B \sin \lambda & \underbrace{r=R \text{ and } r=R-d}_{\text{upper hemisphere}} \\ x_f \frac{\partial V}{\partial x_f} + y_f \frac{\partial V}{\partial y_f} + \left(z_f + \frac{L}{2}\right) \frac{\partial V}{\partial z_f} \\ = \omega(x_f^2 + y_f^2) B \cos \lambda - \omega \left(z_f + \frac{L}{2}\right) x_f B \sin \lambda & \underbrace{r=R \text{ and } r=R-d}_{\text{lower hemisphere}} \end{cases} \quad (18)$$

3. Accounting for the linearity of the Neumann problem the solution potential is split in two parts: a potential V_1 depending on $\cos \lambda$ and a potential V_2 depending on $\sin \lambda$. An analytical solution for V_1 can be found but not for V_2 which is determined through the finite-elements method. The potential is

$$V = \omega \frac{(x_f^2 + y_f^2)}{2} \cos \lambda B + V_2$$

where V_2 is the solution of the reduced Neumann-like problem

$$\begin{cases} \Delta V_2 = 0 \\ x_f \frac{\partial V_2}{\partial x_f} + y_f \frac{\partial V_2}{\partial y_f} = 0 & \underbrace{r=R \text{ and } r=R-d}_{\text{cylindrical part}} \\ x_f \frac{\partial V_2}{\partial x_f} + y_f \frac{\partial V_2}{\partial y_f} + \left(z_f - \frac{L}{2}\right) \frac{\partial V_2}{\partial z_f} \\ = -\omega \left(z_f - \frac{L}{2}\right) x_f B \sin \lambda & \underbrace{r=R \text{ and } r=R-d}_{\text{upper hemisphere}} \\ x_f \frac{\partial V_2}{\partial x_f} + y_f \frac{\partial V_2}{\partial y_f} + \left(z_f + \frac{L}{2}\right) \frac{\partial V_2}{\partial z_f} \\ = -\omega \left(z_f + \frac{L}{2}\right) x_f B \sin \lambda & \underbrace{r=R \text{ and } r=R-d}_{\text{lower hemisphere}} \end{cases} \quad (19)$$

The finite-elements solver gives a value of the torque induced by eddy currents. By linearizing around a reference shape one can find an approached expression of the torque in the body coordinate system.

4. The current density is evaluated with the finite element solver.
5. An approached formula for the torque, reproducing with good accuracy the numerical results obtained by the finite element tool developed in this article is (in the body coordinate system)

$$\vec{T}_b \approx -\underbrace{\frac{\omega B^2}{\kappa} \sin^2 \lambda \left(\pi d L R^3 + \frac{\pi}{3} d R^4 \right)}_{R \sim 1.3 \text{ m } \quad L = 5 \leftrightarrow 7 \text{ m } \quad d \ll R} \vec{e}_k \quad (20)$$

Practically, the approached formula is valid only under the following assumptions: $R \sim 1.3$, L is between 7 m and 5 m and $d \ll R$.

Case 2: capsule rotating along its transverse axis. The same capsule is considered here, but the rotation takes

place about the Ox_f axis, at the angular velocity ω ($\vec{v}_b = -\omega z_b \vec{e}_j + \omega y_b \vec{e}_k$). Once more, self-induction is neglected. The following assumptions are used:

- The magnetic field is constant in the fixed coordinate system and in the xy -plane.
- The capsule is rotating along the e_x axis. The e_x axis and the e_i axis coincide. The e_k axis is the longitudinal axis of the capsule.

The magnetic field is

$$\vec{B}_f(M,t) = B(\cos \lambda \vec{e}_x + \sin \lambda \vec{e}_y)$$

1. From the simplified Ohm's law (8), expressed in the body coordinate system, for a rotating capsule, one gets

$$\begin{cases} \kappa j_i = -\frac{\partial V}{\partial x_b} + \omega z_b \sin \lambda \sin(\omega t)B - \omega y_b \sin \lambda \cos(\omega t)B \\ \kappa j_j = -\frac{\partial V}{\partial y_b} + \omega y_b \cos \lambda B \\ \kappa j_k = -\frac{\partial V}{\partial z_b} + \omega z_b \cos \lambda B \end{cases} \quad (21)$$

2. The Neumann problem is as follows:

$$\begin{cases} \Delta V = 2\omega B \cos \lambda \\ x_b \frac{\partial V}{\partial x_b} + y_b \frac{\partial V}{\partial y_b} = \omega z_b x_b \sin \lambda \sin(\omega t)B - \omega x_b y_b \sin \lambda \cos(\omega t)B + \omega y_b^2 \cos \lambda B & \underbrace{r=R \text{ and } r=R-d}_{\text{cylindrical part}} \\ x_b \frac{\partial V}{\partial x_b} + y_b \frac{\partial V}{\partial y_b} + \left(z_b - \frac{L}{2}\right) \frac{\partial V}{\partial z_b} = \omega z_b x_b \sin \lambda \sin(\omega t)B - \omega x_b y_b \sin \lambda \cos(\omega t)B + \omega y_b^2 \cos \lambda B + \omega z_b \left(z_b - \frac{L}{2}\right) \cos \lambda B & \underbrace{r=R \text{ and } r=R-d}_{\text{upper hemisphere}} \\ x_b \frac{\partial V}{\partial x_b} + y_b \frac{\partial V}{\partial y_b} + \left(z_b + \frac{L}{2}\right) \frac{\partial V}{\partial z_b} = \omega z_b x_b \sin \lambda \sin(\omega t)B - \omega x_b y_b \sin \lambda \cos(\omega t)B + \omega y_b^2 \cos \lambda B + \omega z_b \left(z_b + \frac{L}{2}\right) \cos \lambda B & \underbrace{r=R \text{ and } r=R-d}_{\text{lower hemisphere}} \end{cases} \quad (22)$$

3. Taking advantage of the linearity of Neumann problem, the potential is split into three parts: a time-invariant potential V_1 , a potential V_2 proportional to $\cos(\omega t)$ and a potential V_3 proportional to $\sin(\omega t)$. Analytic solutions for V_1 and V_2 are straightforward, but V_3 must be determined through the finite-elements method. The potential is

$$V(x_b, y_b, z_b) = \frac{B\omega(z_b^2 + y_b^2)\cos \lambda}{2} - \frac{Bx_b y_b \omega \cos(\omega t)\sin \lambda}{2} + V_3$$

where V_3 is the solution of the reduced Neumann

problem

$$\begin{cases} \Delta V_3 = 0 \\ x_b \frac{\partial V_3}{\partial x_b} + y_b \frac{\partial V_3}{\partial y_b} = \omega z_b x_b \sin \lambda \sin(\omega t)B & \underbrace{r=R \text{ and } r=R-d}_{\text{cylindrical part}} \\ x_b \frac{\partial V_3}{\partial x_b} + y_b \frac{\partial V_3}{\partial y_b} + \left(z_b - \frac{L}{2}\right) \frac{\partial V_3}{\partial z_b} = \omega z_b x_b \sin \lambda \sin(\omega t)B & \underbrace{r=R \text{ and } r=R-d}_{\text{upper hemisphere}} \\ x_b \frac{\partial V_3}{\partial x_b} + y_b \frac{\partial V_3}{\partial y_b} + \left(z_b + \frac{L}{2}\right) \frac{\partial V_3}{\partial z_b} = \omega z_b x_b \sin \lambda \sin(\omega t)B & \underbrace{r=R \text{ and } r=R-d}_{\text{lower hemisphere}} \end{cases} \quad (23)$$

As previously described, we can find a linearized approached torque formula through the finite-elements solver.

4. The current density is evaluated with the finite element solver.
5. The approached torque formula in the body coordinate system is

$$\vec{T}_b \approx \underbrace{\frac{\omega B^2}{\kappa} \sin^2 \lambda \left(\frac{3}{4} \pi d L R^3 + \frac{5}{6} \pi d R^4 \right)}_{R \sim 1.3 \text{ m} \quad L = 5 \leftrightarrow 7 \text{ m} \quad d \ll R} \vec{e}_k \quad (24)$$

The approached formula is valid only with the following assumptions: $R \sim 1.3$, L is between 7 m and 5 m and $d \ll R$.

4. Damping of spinning dynamics along orbits of interest

4.1. Description of interesting orbits and its environmental conditions

We now study debris from Ariane 4 upper stages. Those stages, called H10, were initially in Sun-synchronous orbits with altitudes ranging from 500 to 800 km; therefore the orbit inclination is approximately $97\text{--}98^\circ$. We use the IGRF 2005 (with the 2010 coefficients) magnetic model to simulate the internal Earth magnetic field without modeling the time variation (time variation does not change the value of the magnetic field more than 0.1% in a year). This model gives us the direction and the intensity of the magnetic field at each point along the orbit. Fig. 3 shows orientation and absolute value of the magnetic field vector along a typical trajectory computed with the IGRF model.

The intensity of the magnetic field for a typical H10 orbit ranges from 0.1 G at equator up to 0.55 G at poles. The air drag torque is neglected and it is assumed that passivation is already accomplished, so one can ignore fuel friction in tanks. The only torque besides the eddy current torque is the gravity gradient torque.

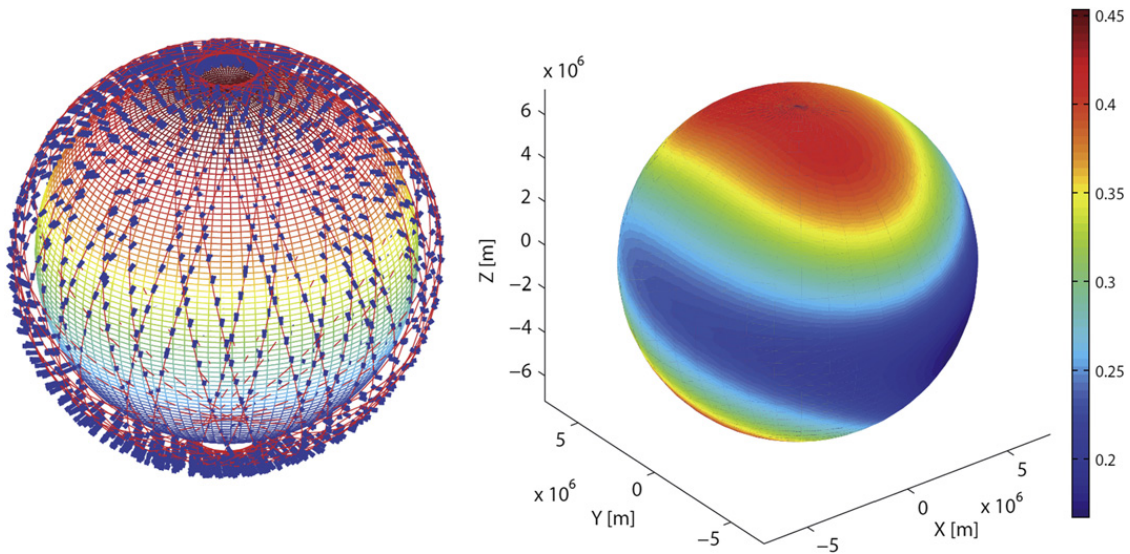


Fig. 3. Stages trajectory, orientation and intensity of the magnetic field encountered.

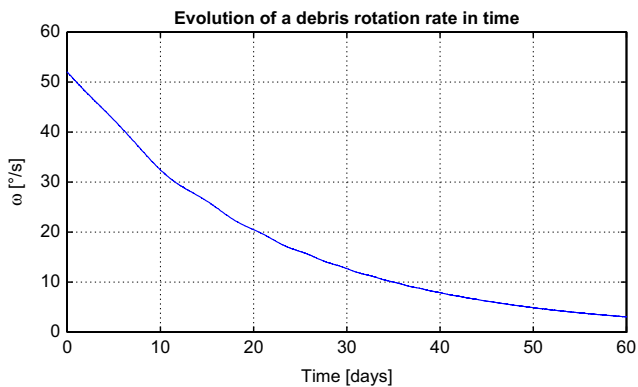


Fig. 4. Attitude simulation for the flight V35 H10 stage (axial spin as initial condition).

4.2. Axial spin case

The attitude dynamic of a debris subject to gravity gradient and eddy current torques is now simulated. It is assumed that the longitudinal axis of the debris coincides with its linear velocity vector. The debris is rotating along this axis with an angular velocity ω_0 . These two assumptions represent initial attitude conditions for the debris. The attitude dynamic equation reads

$$\dot{\vec{\omega}} = \vec{I}^{-1} (\vec{T} - \vec{\omega} \times \vec{I} \vec{\omega}) \quad (25)$$

where $\vec{T} = \vec{T}_{gg} + \vec{T}_{ec}$, \vec{T}_{gg} represents the gravity gradient torque and \vec{T}_{ec} the eddy current torque. In the body coordinate system, this torque is equal to

$$\vec{T}_{ec} = \begin{pmatrix} -\frac{1}{\kappa} \left(\pi d L R^3 + \frac{\pi}{3} d R^4 \right) \omega_i (B_j^2 + B_k^2) \\ -\frac{1}{\kappa} \left(\frac{3}{4} \pi d L R^3 + \frac{5}{6} \pi d R^4 \right) \omega_j (B_i^2 + B_k^2) \\ -\frac{1}{\kappa} \left(\frac{3}{4} \pi d L R^3 + \frac{5}{6} \pi d R^4 \right) \omega_k (B_i^2 + B_j^2) \end{pmatrix}_b \quad (26)$$

where (B_i, B_j, B_k) are the components of the Earth magnetic

Table 3
Axial spin simulation results.

Flight	Za (km)	Zp (km)	ω_0 ($^\circ/s$)	Damping time cst.(days)
V35	779	764	52	25
V44	764	760	60	25
V52	798	782	38	22
V72	774	766	39	25
V75	625	594	60	19
V107	789	783	37.5	22
V124	623	610	42	23

Table 4
Flat spin simulation results.

Flight	ω_0 ($^\circ/s$)	Damping time cst. (days)
V52	20	190
V107	20	225

field in the body system of coordinates and $(\omega_i, \omega_j, \omega_k)$ the components of $\vec{\omega}$ in the same system of coordinates.

Fig. 4 shows the results for the debris of the Ariane flight 35 and $\omega_0 = 52^\circ/s$ (this is approximately the speed rotation measured for this H10 stage). The inertia tensor used for this simulation is taken from Ariane 4 datasheet [5]. The rotation speed exponentially decreases as has been observed for other space bodies. This simulation illustrates the phenomenon of eddy current rotation damping. Table 3 contains the results of other simulations. All simulations show identical exponentially decreasing trends. The evaluated decay time concerning an H10 stage ranges from 19 to 25 days.

4.3. Flat spin case

The axial spin case is of particular interest as it corresponds to the initial rotation configuration. Due to multiple factors, e.g. fuel friction in tanks, the initial axial spin configuration is unstable and may rapidly change to

a flat spin configuration [18]. To evaluate the time of decay, the same torque equation (26) is used. The rotation also exponentially decreases but the time of decay is much longer than the axial spin configuration as pointed out in Table 4.

4.4. Damping time constant

Whatever the rotation configuration under consideration, an eddy current torque is induced in a conducting body rotating in a homogeneous magnetic field. The simulation of the attitude dynamic equation for an aluminum H10 stage in LEO shows the expected exponential decrease on the angular rate. The time of decay is strongly related to the rotation configuration but is, in all cases, below 250 days. At the light of these simulations and the few observations that have been reported in the literature (e.g. [17] or [1]), one can expect to find conducting debris with very low angular rates after having spent a few years in near-Earth space.

5. Observation of debris motion

A natural next step in the study of the residual motion of old debris in orbit is direct observation. To validate the results presented above and to verify that one can expect the targets for Active Debris Removal to be relatively steady, therefore easily catchable, these observations are needed. Such observations can be done in situ, with orbital assets approaching the target and being observed with optical or radar means, or can be operated from the ground, again with optical or radar means.

Currently, there exists no orbital system capable of monitoring the movement of satellites (or at least such results have not been published, up to our knowledge). Therefore, the only remaining possibility is ground observations.

5.1. Radar observation

Numerous radars are suitable for the observation of the debris. One of the most efficient is the TIRA (Tracking & Imaging Radar) from FGAN (Forschungsgesellschaft für Angewandte Naturwissenschaften), in Germany; it is capable of providing kinematics of large objects with a precision in the range of 0.1°/s in all directions, as was mentioned for instance by Kawamoto et al. [8].

The French ship “Le Monge” could make several observations of a selected batch of old Ariane upper stages. The requirements are to have two observation periods per object lasting more than 5 min with an accuracy better than 1 s, with different sight angles to guarantee a good 3D resolution.

These series of observations have effectively been performed at the end of May 2011, considering two upper stages, corresponding to the Ariane flights V75 and V107 shown in Table 3. These upper stages had initial rotation velocities of respectively 60°/s and 37.5°/s. The observations will be studied subsequently.

Table 5
Synthesis of observations devoted to old Ariane upper stages [6].

Name	Launch	Za (m)	Zp (m)	i (°)	Obs.	Movement	Magnitude	Last Obs.	Remarks
ARIANE 5 R/B V165	18/12/2004	705,298	570,330	98.31	1	S	+2.5	23/06/2005	First obs period 39s, 4th obs almost S
ARIANE 5 R/B V145	01/03/2002	797,761	749,554	98.18	7	S	+4 to +5.5	17/09/2005	
ARIANE 40 R/B V124	03/12/1999	620,639	609,394	98.12	1	S	4	16/01/2005	Two obs. almost S Initial periods 45–90 s then S
ARIANE 40 R/B V107	24/03/1998	787,823	782,406	98.25	14	S	+2 to +5	10/09/2000	
ARIANE 40+3 R/B V75	07/07/1995	622,743	592,284	98.28	4	S or almost S	+4 to +5	17/04/1999	Fourth obs. S or long Two obs. variable, period 60 s Rapidly varying 12 s then almost S
ARIANE 40+ R/B V72	21/04/1995	775,265	764,971	98.52	52	Variable to S	+2.5–7	07/12/2001	
ARIANE 40 R/B V59	26/09/1993	798,394	781,406	98.66	10	S	+3 to 5	11/02/1999	Rapidly varying 20 s then S Tumbling (breakup) then S
ARIANE 42P R/B V52	10/08/1992	1,408,489	1,292,382	66.06	5	Undetermined	+3.5–8	02/05/1994	
ARIANE 40 R/B V44	17/07/1991	762,516	759,238	98.72	61	S at the end	+3.5–8	04/09/2005	
ARIANE 40 R/B V35	22/01/1990	777,352	763,655	98.67	24	S at the end	+4.3–6	06/09/1997	
ARIANE 1 R/B V16	22/02/1986	797,522	781,000	98.89	6	S at the end	+3–7	28/08/2007	

5.2. Amateur observations

Several networks of amateur astronomers publish their observations on the Internet. A typical and very rich example is given in [6]. The provided information details the observation conditions, dates, azimuths, magnitude and magnitude variation. They also provide a qualitative information relative to the movement of the object. For example, the Ariane upper stage of flight V75 has been reported four times, with normalized magnitudes between 4 and 5, and a movement quoted as “Steady” or “Almost Steady”. Table 5 gives a synthetic view of the behavior of Ariane upper stages present in low Earth orbit, according to [6]. It describes, from left to right, the name of the debris and its launch date, the orbital parameters (apogee height, perigee height, inclination), the number of reported observations, the magnitude and its variability, the date of last observation, and general comments on the movement of the debris. From this table, one can see that the vast majority of the debris are noted as “Steady” or “Almost Steady”. Unfortunately, these qualitative observations are not really quantified. Further, most of the observations are relatively old, most of them having been performed shortly after the launch.

Nevertheless, it seems obvious that they corroborate the model of “magnetic damping” of the rotational movement of the debris discussed in this paper.

6. Conclusion

The number of pieces of space debris has emerged as a serious threat to the future of space programs. Numerous solutions to limit the number of debris in low Earth orbit are under study but one of the major problems in the development of such solutions concerns the angular rate of the debris. In this paper, we have introduced a general model of the induction phenomenon yielding an exponential damping of the spin motion for a conducting piece of space debris the Earth magnetic field. A calculation method for this damping has been applied to an aluminum H10-stage-like shape. The evaluated eddy-current braking torque has been used in an attitude simulator in a low Earth orbit to evaluate the damping time constant of a typical H10 stage which is evaluated to be lower than 250 days.

The previous papers on the subject [1,4,14,15,17], the few observations and the results of this analysis all indicate a natural angular rate damping of a conducting debris in low Earth orbit. The damping time constant is strongly related to the debris shape, material and rotation properties but the results of this analysis strongly suggests that one can expect debris to have only low angular rates after few years in space.

Acknowledgements

This study was performed under R&T CNES Contract.

The authors wish to thank CNES for financial support, and David Vissière and Pierre-Jean Bristeau from SYSSNAV for their technical support.

References

- [1] H. Boehnhardt, H. Koehnke, A. Seidel, The acceleration and the deceleration of the tumbling period of Rocket Intercosmos 11 during the first two years after launch, *Astrophys. Space Sci.* 162 (2) (1989) 297–313.
- [2] R. Dautray, J.-L. Lions, *Mathematical Analysis and Numerical Methods for Science and Technology*, vol. 1, Springer Verlag, Berlin, 1990.
- [3] PDE solver, version 3.17-0 <<http://www.freefem.org/ff++/index.htm>>, June 2011.
- [4] H. Hertz, *On Induction in Rotating Spheres*, Miscellaneous Papers, Macmillan and Co. Ltd, 1896.
- [5] Dossier de définition Troisième étage H10 III, A4-DF-1300000-D, AEROSPATIALE ESPACE & DEFENSE, 1994.
- [6] Amateur observations <<http://www.io.com/mmccants/ppas/index.html>>, June 2011.
- [7] Y. Ishige, S. Kawamoto, S. Kibe, Study on electrodynamic tether system for space debris removal, *Acta Astronaut.* 55 (11) (2004) 917–929.
- [8] S. Kawamoto, Y. Ohkawa, S. Nishida, S. Kitamura, S. Kibe, T. Hanada, M. Mine, Strategies and technologies for cost effective removal of large sized debris, in: International Conference on Orbital Debris Removal, Westfields Marriott, Chantilly, VA, USA, Oral Presentation, 8 December 2009, 2004.
- [9] D.J. Kessler, G. Burton, Collision frequency of artificial satellites: the creation of a debris belt, *J. Geophys. Res.* 83 (A6) (1978) 2637–2646.
- [10] V. Lappas, N. Adeli, J. Fernandez, T. Theodorou, L. Visagie, H. Steyn, O. Le Couls, M. Perren, Cubesail: a low cost small cubesat mission for de-orbiting LEO objects, *Small Satell. Syst. Serv.* (2010).
- [11] N. Lebedev, I.P. Skalaskaya, Y.S. Uflyand, *Worked Problems in Applied Mathematics*, Dover Publications, 1979.
- [12] J.-C. Liou, N.L. Johnson, N.M. Hill, Controlling the growth of future LEO debris populations with active debris removal, *Acta Astronaut.* 66 (5–6) (2010) 648–653.
- [13] J.M. Ruault, M.C. Desjean, C. Bonnal, P. Bultel, Active Debris Removal (ADR): from identification of problematics to in flight demonstration preparation, in: 1st European Workshop on Active Debris Removal, Paris, France, Oral Presentation, 22 June 2010.
- [14] G.L. Smith, *A Theoretical Study of the Torques Induced by a Magnetic Field on Rotating Cylinders and Spinning Thin Wall Cones, Cone Frustrums, and General Bodies of Revolution*, NASA, TR-R-129, 1962.
- [15] W.R. Smythe, *Static and Dynamic Electricity*, second ed., McGraw-Hill, London, 1950 (p. 417).
- [16] J.R. Wertz, *Spacecraft Attitude Determination and Control*, Astrophysics and Space Science Library, Kluwer Academic Publishers, 1980 (p. 501).
- [17] R.H. Wilson Jr., Magnetic effects on space vehicles and other celestial bodies, *Ir. Astron. J.* 13 (1/2) (1977) 1–13.
- [18] Etude de la stabilité de la nutation du H 140 après séparation avec L5 ou Hermes, Flat-Spin H 140, A5-NT-1-133, AEROSPATIALE, 1987.
- [19] T.S. Kelso, Analysis of the IRIDIUM 33-COSMOS 2251 collision, in: AIAA/AAS Astrodynamics Specialist Conference, Oral Presentation, August 2009.
- [20] J. Starke, B. Bischof, W.-O. Foth, J. Günther, ROGER a potential orbital space debris removal system, in: 38th COSPAR Scientific Assembly, Bremen, Germany, Oral Presentation, 18–15 July 2010.